Learning Weather-General and Weather-Specific Features for Image Restoration Under Multiple Adverse Weather Conditions

Yurui Zhu [1, 3, ⋆, †], Tianyu Wang [2, †], Xueyang Fu [1, ✉], Xuanyu Yang [3, ⋆],
Xin Guo [1], Jifeng Dai [4, 3], Yu Qiao [3], Xiaowei Hu [3, ✉]
[1] University of Science and Technology of China [2] The Chinese University of Hong Kong
[3] Shanghai Artificial Intelligence Laboratory [4] Tsinghua University
zyr@mail.ustc.edu.cn, xyfu@ustc.edu.cn, huxiaowei@pjlab.org.cn

Abstract

Image restoration under multiple adverse weather conditions aims to remove weather-related artifacts by using a single set of network parameters. In this paper, we find that image degradations under different weather conditions contain general characteristics as well as their specific characteristics. Inspired by this observation, we design an efficient unified framework with a two-stage training strategy to explore the weather-general and weather-specific features. The first training stage aims to learn the weather-general features by taking the images under various weather conditions as inputs and outputting the coarsely restored results. The second training stage aims to learn to adaptively expand the specific parameters for each weather type in the deep model, where the requisite positions for expanding weather-specific parameters are automatically learned. Hence, we can obtain an efficient and unified model for image restoration under multiple adverse weather conditions. Moreover, we build the first real-world benchmark dataset with multiple weather conditions to better deal with real-world weather scenarios. Experimental results show that our method achieves superior performance on all the synthetic and real-world benchmarks. Codes and datasets are available at this repository.

1. Introduction

Adverse weather conditions, such as rain, haze, and snow, are common climatic phenomena in our daily life. They often lead to the poor visual quality of captured images and primarily deteriorate the performance of many outdoor vision systems, such as outdoor security cameras

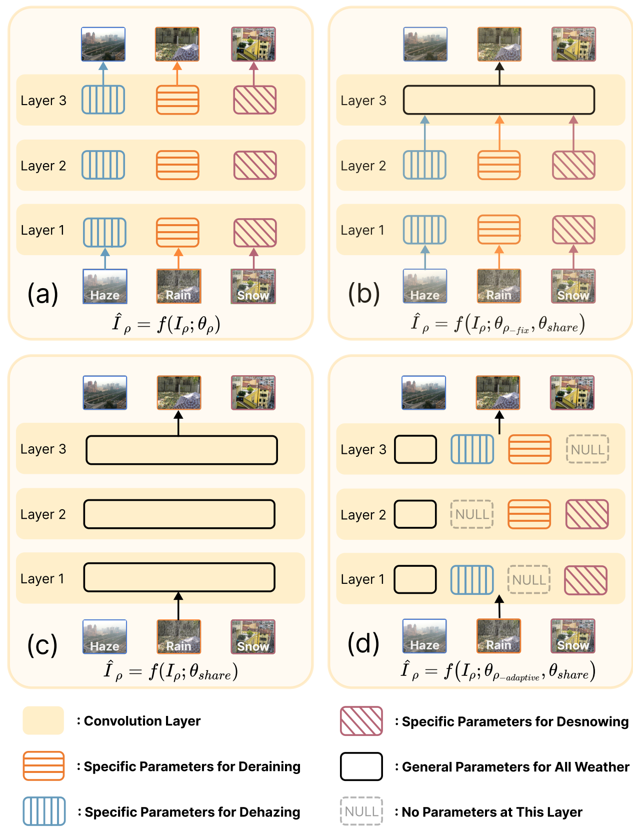

Figure 1. Illustration of the proposed method and the currently existing solutions. (a) The weather-specific methods; (b) the method of [41]; (c) methods of [6, 69]; (d) our method, which learns the weather-specific and weather-general features in an efficient manner to remove multiple weather-related artifacts.

and automatic driving [53, 107]. To make these systems more robust to various adverse weather conditions, many restoration solutions have been proposed, such as deraining [16, 17, 25, 40, 72, 73, 82, 83], dehazing [1, 23, 49, 65, 80, 84], desnowing [4, 51, 97], and raindrop removal [22, 59, 96].

⋆ : This work was done during their internship at Shanghai Artificial Intelligence Laboratory.
† : Co-first authors contributed equally.
✉ : Corresponding authors.

Albeit these approaches exhibit promising performance in the given weather situation, they are only applicable to certain typical weather scenarios. However, it is inevitable to tackle various kinds of weather in the application of outdoor vision intelligent systems. Consequently, as shown in Fig. 1 (a), multiple sets of weather-specific model parameters are required to deal with various conditions, which brings additional computational and storage burdens. Hence, it is vitally requisite to develop a unified model capable of addressing various types of adverse weather conditions via a single set of network parameters.

Recently, several methods [6, 41, 69] adopt a single set of network parameters to remove different weather-related artifacts. However, these solutions contain limitations for practical deployment and applications. Firstly, some methods [6,69] fail to consider the specific characteristics of each weather condition in their proposed unified models, limiting their restoration performance on specific weather conditions. Secondly, as shown in Fig. 1 (b), although Li *et al*. [41] tackle the differences and similarities of weather degradation with multiple individual encoders and a shared decoder. Such multiple fixed encoders may largely increase network parameters. Thirdly, existing unified models [6, 41, 69] often require a large number of parameters, limiting the model efficiency. Lastly, current state-of-the-art methods [6, 41, 69] mainly employ synthesized datasets in their training phase, causing apparent performance drops in real-world scenarios.

In this paper, we argue that images with different weather distortions contain general characteristics as well as their specific characteristics. According to the atmosphere scattering model [55, 57], due to the attenuation and scattering effects, these weather disturbances often share some similar visual degradation appearances, *e.g*., low contrast and color degradation. Meanwhile, the typical type of weather distortion has its unique characteristics. For example, rainy images often suffer from occlusion by rain steaks with different shapes and scales [32, 82]; haze exhibits global distortions on the entire images [34, 65]. Pioneer works also have devised many specific priors [23, 72, 80, 83, 97] for different weather conditions, which motivates us to explore *weather-general* and *weather-specific features* to perform image restoration under multiple weather conditions.

To achieve this, we design an efficient unified framework for multiple adverse weather-related artifacts removal by exploring both weather-general and weather-specific features. The training procedure of our framework consists of two stages. The first training stage aims to learn the general features by taking various images under different weather conditions as the inputs and outputting coarse results for multiple weather conditions. In the second training stage, we devise a regularization-based optimization scheme, which learns to adaptively expand the specific parameters for each weather type in the deep model. Note that these requisite positions to expand weather-specific parameters could be learned automatically, thus avoiding redundant parameters pre-designed by researchers. Hence, we are able to obtain an efficient and unified model for image restoration under multiple adverse weather conditions. Furthermore, we newly construct the first real-world benchmark dataset with multiple weather conditions to better deal with various weather-related artifacts in real-world scenarios.

The contributions of this paper could be summarized as:

- We reveal that image degradations under different weather conditions contain both general and specific characteristics, which motivates us to design a unified deep model by exploring the weather-general and weather-specific features for removing weather-related artifacts under multiple weather conditions.

- We present a two-stage training strategy to learn the weather-general and weather-specific features automatically. Moreover, the weather-specific features are adaptively added at the learned positions, which makes our model efficient and effective.

- In order to better deal with real-world weather conditions, we construct the first real-world benchmark dataset with multiple weather conditions. Additionally, experimental results validate the superiority of our proposed method on various benchmarks.

2. Related Work

Single image restoration under different weather conditions have been extensively studied in previous literatures, including deraining [16, 17, 19, 25, 26, 32, 40, 43, 72, 73, 78, 79, 82, 83, 86, 95, 104], dehazing [1, 10, 12, 23, 45, 49, 50, 65, 80, 84, 90, 98], desnowing [4, 51, 97], and raindrop removal [22, 59, 62, 96].

Rain removal. The effects of rainy weather on images are usually divided into rain streaks and rain drops. For rain streak removal, [16] first applies the convolutional neural network on deraining, followed by GAN [94] and recurrent network [43]. Researchers look for better ways to understand and represent rain streaks [2, 7, 32, 40, 74, 81, 91, 101, 106], for more delicate detail recovery [11, 89], and for wider applicability under severe weather condition [40, 82]. Besides, many studies introduce the adversarial learning [40], transfer learning [27, 87], frequency priors [21, 28, 29, 103] and data generation to improve the models' performance.

The degradation of raindrops is different from that of streaks. Thus, they are usually treated separately. There are approaches including CNN [15], attention map [59], and mathematical descriptions [22, 63] on raindrop removal.

Haze removal. [23] proposes a simple prior of hazy images. [1, 65, 93] applies various methods for dehazing, followed by GAN [61, 84] and fusion-based strategy [66], attention-based model with trainable pre-treatment part [49], dense feature fusion [13], and the combination of CNN and transformer [20]. [38, 80] consider various priors and modeling of raindrops. Proposed learning methods include contrastive regularization [77] and multi-guided bilateral learning [102]. [44] pays attention to colorful haze removal. There are also works pursuing stronger utilization and generalization on datasets [8, 46, 85].

Snow removal. [51] designs a two-stage network to deal with different types of snow, while [4] considers the veiling effect. [31] proposes a pyramid-structure model with lateral connections. [5] uses dual-tree wavelet transform. [97] introduces semantics and depth prior to snowfall removal.

Multiple weather-related artifacts removal. Different from the above typical single weather removal task, all-weather-removal is required to recover the clear images with a single set of network parameters under multiple kinds of weather conditions. Moreover, due to the differences among different tasks, all-weather-removal is obviously more challenging than the single image restoration task. Li *et al*. [41] explore the differences and similarities of each weather degradation by designing an all-in-one network with multiple encoders. [6] combines the two-stage knowledge and multi-contrastive learning strategy to handle the weather removal problem. [69] propose a transformer-based network with learnable specific weather queries to handle the weather removal in a unified model. The method [41] and our method both consider the differences and similarities among different weathers. However, unlike [41] using the specific weather parameters at the fixed encoder positions, our method could adaptively expand the specific parameters for a certain weather type at the learned network positions, which is more flexible and efficient.

Multi-task learning (MTL). MTL mainly focuses on handling multiple tasks in a single network, which is extensively studied in the high-level [48, 71, 100, 105] and low-level vision tasks [3, 42]. Recently, methods [3, 42] attempt to exploit the transformers and pre-training scheme to handle multiple image restoration tasks, including deraining, denoising, and super-resolution. However, the correlation among these tasks is limited, while different weather degradations exist with apparent similarities to a certain extent.

3. Motivation

Weather-distorted images are often captured in outdoor environments. Here, we would like to further analyze the general and specific characteristics of different weather conditions from the following two perspectives.

The degradation in bad weathers. Different weather effects, *i.e*., rain, haze, and snow, are mainly caused by the various particles involved in the transparent medium (air space) based on the atmosphere optics. The atmosphere scattering model [54, 56] describes the imaging formulation in bad weather conditions, which reveals that the received irradiance of a certain scene point from the photographic sensor is the summation of the direct transmission (attenuation) and the airlight, respectively:

$$E = \underbrace{E_\infty \rho e^{-\beta d}}_{\text{Direct transmission}} + \underbrace{E_\infty \left(1 - e^{-\beta d}\right)}_{\text{Airlight}}, \quad (1)$$

where E_∞ denotes the sky intensity; ρ denotes the normalized radiance of the certain scene point; βd denotes the optical distance of a certain scene point. Here we refer readers to [55–57] for more details. In Fig. 2 (a), we also provide the illustration of Eq. (1), in which the former term (direct transmission) describes the attenuation effect of the object light travel through the atmosphere, and the latter term (airlight) reveals the scattering of illumination by different involved particles in the atmosphere space.

According to the above physical imaging model, different weather effects share general characteristics. In detail, during the imaging process, particles of different weathers unavoidably modulate the light transmitting from the certain scene point to the sight of observers. The scattering light integration along the light propagation path [54] may unavoidably change the brightness of different weather conditions (Fig. 2 (b)). Thus, images under different adverse weathers exist common degradation, such as low contrast and subtle color distortion.

Besides, there also exist weather-specific characteristics

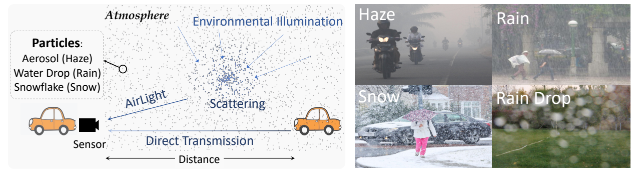

(a) (b)

Figure 2. (a) Illustration of the atmosphere scattering model [54, 56] in various weather conditions. (b) Real-world scenes of different weather conditions.

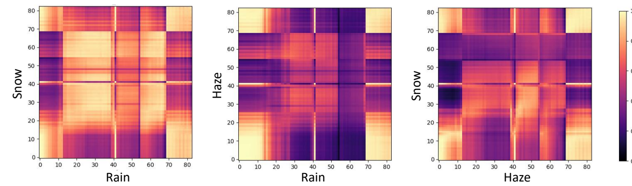

(a) (b) (c)

Figure 3. Similarity visualizations among different layers of multiple pre-trained models for deraining, dehazing, and desnowing. (a) The similarity of Rain and Snow models; (b) the similarity of Rain and Haze models; (c) similarity of Haze and Snow models. The values on two axes (0-80) indicate the position order of different network layers, where we uniformly sampled 80 layers.

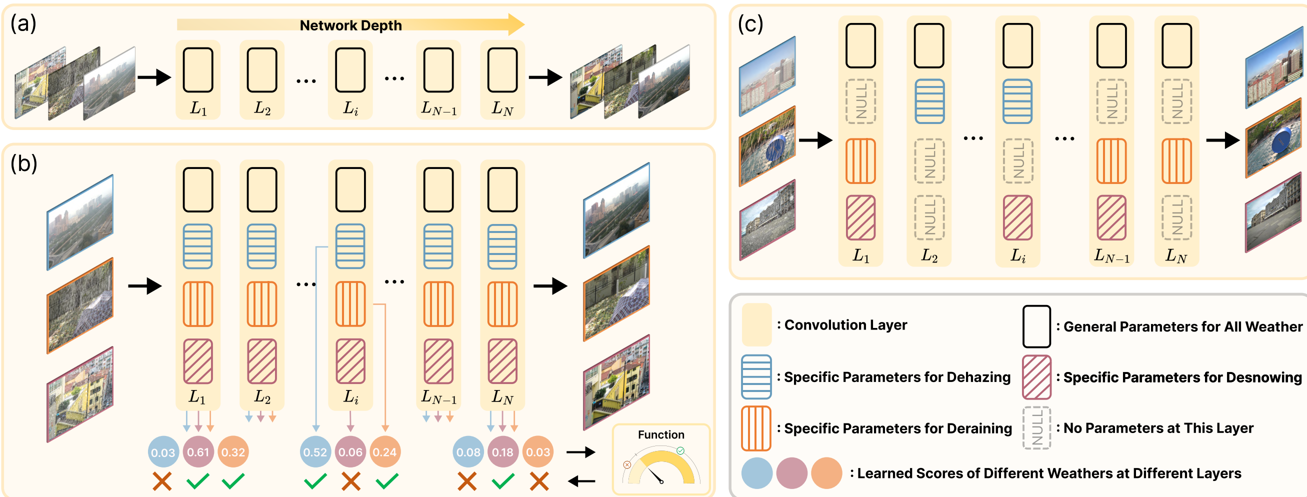

Figure 4. The overall illustration of our method. (a) and (b) illustrate the first and second training stages of our framework, respectively; (c) illustrates the inference stage of our framework. For simplicity, skip connections are omitted.

in each weather condition. For instance, the particle type of haze is aerosol, and haze is assumed as the entire image corruption [1,68]. Rain is constituted of water drops, and rainy images suffer from occlusion by the large motion-blurred particles with different shapes and scales. In contrast, irregular particle trajectories and opaque snowflakes are commonly seen in snowfall images. These differences among multiple weather types will cause interference when removing multiple weather-related artifacts. Hence, many more accurate physical models [4, 39, 75, 81] of various weather conditions based on Eqn. 1 are appeared, which further incorporate the typical weather priors into their models.

Analysis of feature representations. To study the feature representations in deep networks for different weather-related artifacts removal, we individually train the models on different weather datasets using the UNet-based structure network [67]. Then, we adopt centered kernel alignment (CKA) [9, 36, 37, 42, 58] to measure the similarity of feature representations in deep networks, which have been pre-trained on the different weather datasets.

The similarity visualizations across hidden layers of different networks are shown in Fig. 3. The internal representations learned on the rain dataset seem similar to the counterparts on the snow dataset. One plausible reason is that many snowfall images often resemble rainy images regarding appearances of degradation. While from Fig. 3 (b) and (c), the layers of the dehazing model have more similar patterns to the layers of deraining or desnowing models at the shallow and deep layers. Although networks are trained with different weather datasets, similar representations still exist at the sub-set of network positions.

Above observations motivate us to expand parameters for different weather types in an adaptive manner, which is flexible and efficient for multiple weather artifacts removal.

4. Methodology

To explore weather-specific and weather-general features for multiple weather removal tasks, we construct a unified network architecture based on the U-Net [67]. Additionally, as shown in Fig. 4, we devise a novel two-stage training strategy, where we separately learn weather-general features and weather-specific features in the first and second training stages. Then, we elaborate the implementation details of our method. Without loss of generality, we assume that weather types include rain, snow, and haze.

4.1. Weather-General Feature Learning

We employ the shared backbone network to learn the weather-general features. Specifically, various types of weather images are adopted to jointly update the shared backbone network, which helps the network to learn the weather-general feature representations. The forward process at this stage could be formulated as

$$\hat{X}_\rho \ = \ f\left(X_\rho; \theta_{share}\right) \ , \tag{2}$$

where X_ρ and $\hat{X}_\rho$ denote the input and recovered images of weather type ρ; θ_{share} denotes the general sharing parameters for all weather types, which are jointly optimized by multiple weather datasets.

In addition, the aforementioned Eq. (1) reveals that the bad weather degradation is largely related to the depth of corresponding scenes. Hence, we introduce the depth information in our framework to optimize the network. We adopt the depth consistency loss L_{depth}, which fully exploits the general depth auxiliary information among different adverse weathers. Hence, the final loss function of the first training stage is formulated as follows:

$$\mathcal{L}_{s1} \ = \ L_{content}(\hat{X}_\rho, Y_\rho) + \lambda_{depth}||D(\hat{X}_\rho) - D(Y_\rho)||_1 \ , \tag{3}$$

where $L_{content}$ denotes the L1 and perceptual losses [33]; $\hat{X}_\rho$ and Y_ρ indicate the outputs and labels of the weather ρ; $D(\cdot)$ denotes the pre-trained depth estimation network [47], and λ_{depth} denotes the balanced weight.

4.2. Weather-Specific Feature Learning

Adopting the shared parameters to deal with different weather conditions often degrades the restoration performance on each weather due to the interference issues of different sub-tasks. A straightforward solution is to insert the specific parameters for each weather condition across the network layers. Without loss of generality, such network expansion manner of the specific parameter θ_ρ for the weather type ρ ($\rho \in [Rain, Haze, Snow]$) is defined as

$$\theta_\rho^i = \theta_{share}^i + \Delta\theta_\rho^i \,, \tag{4}$$

where θ_{share}^i denotes the general sharing weights at the network layer i; $\Delta\theta_\rho^i$ denotes the specific weights of weather type ρ at the layer i ($i = 1, 2, \dots, N$, N is the total number of network layers).

However, such a simple and fixed network expansion paradigm exists limitations. First, according to the analysis in Sec. 3, the fixed form of expansion for different weathers is redundant and inflexible, leading to heavy computation overhead. Second, when the weather types increase, the fixed expansion manner will introduce the massive network parameters. A problem naturally arises: *how to efficiently and flexibly explore weather-specific features to boost the network performance on a certain weather type?*

In this regard, we devise the regularization-based optimization scheme to achieve adaptive weather-specific parameters expansion for different weather types. In detail, we take the pre-trained model at the first stage as the basic model, where the parameters (θ_{share}) are shared in different weather conditions. To learn the weather-specific features, we first keep the parameters θ_{share} frozen during this second training stage. Then, we introduce the weather-specific parameters $\Delta\theta_\rho$ and learnable scoring variable S_ρ^i for the typical weather ρ at the network layer i. Hence, in our method, the parameters of the typical weather type ρ at the layer i could be reorganized as

$$\theta_\rho^i = \theta_{share}^i + F_\tau(S_\rho^i) * \Delta\theta_\rho^i \,, \tag{5}$$

where S_ρ^i is the learnable scoring variable, which is used to assess the necessity to expand parameters at the layer i. An indicator function $F_\tau(\cdot)$ is designed to determine whether to add the new parameters or not, which is defined as

$$F_\tau(S_\rho^i) = \begin{cases} 1 & \text{if } S_\rho^i \geq \tau \,, \\ 0 & \text{otherwise} \,, \end{cases} \tag{6}$$

where τ is the threshold hyperparameter. Only if S_ρ^i is larger than the threshold τ, the new parameters will be allowed to add to the deep network. Here, we study the convolution operators with the kernel sizes of 1×1 or 3×3 as the newly added weather-specific parameters (please see Sec. 6.4 for the detailed ablation study).

Lastly, the overall loss function of the second training stage could be formulated as follows:

$$\mathcal{L}_{s2} = \sum_\rho \left(L_{content}(\hat{X}_\rho, Y_\rho) + \lambda_{reg} \sum_{i=1}^{N} \left| S_\rho^i \right|_1 \right) , \tag{7}$$

where $L_{content}$ denotes the MAE and perceptual losses [33]; $\hat{X}_\rho$ and Y_ρ indicates the restored outputs and ground truths of the weather ρ; λ_{reg} denotes the hyperparameter of the regularization term. As described in Eq. (7), we introduce the sparsity regularization of S_ρ^i in the objective functions, which guides the network to automatically discover the network positions where we need to add weather-specific parameters. Experimental results also reveal that adding relatively small weather-specific parameters to the learned positions will significantly improve model performance (see Sec. 6.4 for details). Therefore, our network could flexibly learn the weather-specific parameters and efficiently handle various weather conditions.

4.3. Inference Stage

Fig. 4 (c) illustrates the inference stage of our method. The learned model comprises the weather-general parameters for different weathers and the adaptive weather-specific parameters for each typical weather at the sub-set of network positions. For example, taking an image with a certain type of weather (*e.g.*, haze) as the input, the image will pass through the parameters in black and blue color. Note that these positions marked "NULL" indicates that these parameters are unnecessary and the forward propagation will not pass through these layers.

5. Real-World Datasets for Multiple Weather-Related Artifacts Removal

Current all-weather-removal approaches rely on synthetic datasets to train their models, which limits their generalization capability to deal with real-world scenarios. To this regard, we construct the first real-world benchmark datasets under various weather conditions, including haze, rain, and snow. For dehazing, we directly employ the existing real-world dehazing dataset [99]. For deraining, we construct the SPA+ dataset based on the previous SPA [73] dataset. SPA is the first large-scale real-world dataset with paired images. However, SPA still contains two evident issues: (i) many images with sparse rain steaks and repeated background scenes; and (ii) existing images with the same scenes in both training and testing sets. To solve these issues, we first merge the images with repeated background scenes and densify the rain streaks. Then, we remove the images with the same scenes from the training set.

Figure 5. (a) and (b) illustrate the visual samples of the real-world dehazing dataset [99] and our proposed $RealSnow$, respectively. (c) exhibits the same scenes with sparse rains occur multiple times in SPA and corresponding merged images in our proposed SPA+.

Table 1. Illustration of three dataset settings for the weather removal task (R: Rain; RD: RainDrop; S: Snow; H: Haze).

Setting	Weather Types	Datasets	Training Configurations
[Setting 1] (Synthetic)	(R, RD, H)	Outdoor-Rain [40] RainDrop [59] Snow100K [51]	Uniformly sampling 9000 images pairs
[Setting 2] (Synthetic)	(R, S, H)	Rain1400 [17] RESIDE [39] Snow100K [51]	Uniformly sampling 5000 images pairs
[Setting 3] (Real)	(R, S, H)	SPA+ $RealSnow$ REVIDE [99]	Uniformly sampling 160000 images patches

In addition, inspired by [73], we build the first real-world desnowing dataset by using the background-static videos to acquire real-world snowing image pairs. The proposed real-world snow dataset, named $RealSnow$, has 1890 image pairs in total, where 1650 image pairs are used for training, and 240 image pairs are for evaluation. These images are acquired from 126 background-static videos with a wide variety of urban or natural background scenarios, *e.g.*, buildings, cars, statues, trees, and roads. These scenes include varying degrees of snowfall densities and illuminations (*e.g.*, day and night). $RealSnow$ also contains various resolutions, and the average resolution is 1208×646. The example images from our dataset are shown in Fig. 5.

6. Experiments

6.1. Implementation Details

We implement our method on Pytorch platform. Adam optimizer [35] is adopted. At the first stage, our model is trained for 100 epochs, and the initial learning rate is 2×10^{-4}, which is adjusted with the cosine annealing scheme [52]. In the second stage, our model is trained for another 100 epochs, and the initial learning rate is 1×10^{-4}, which is also adjusted with the cosine annealing scheme. The patch size is set as 224×224. Additionally, hyperparameters are empirically set as: $\tau = 0.1$, $\lambda_{depth} = 0.02$, and $\lambda_{reg} = 0.08$.

Table 2. **[Setting 1]** Comparisons on the Outdoor-Rain [40].

Type	Method	Venue	PSNR ↑	SSIM ↑
Deraining	pix2pix [30]	*CVPR' 17*	19.09	0.71
	HRGAN [40]	*CVPR' 19*	21.56	0.86
	MPRNet [92]	*CVPR' 21*	21.90	0.85
Multi-Tasks	All-in-One [41]	*CVPR' 20*	24.71	0.90
	TransWeather [69]	*CVPR' 22*	23.18	0.84
	Chen *et al*. [6]	*CVPR' 22*	23.94	0.85
	Ours	-	25.31	0.90

Table 3. **[Setting 1]** Comparisons on the RainDrop dataset [59].

Type	Method	Venue	PSNR ↑	SSIM ↑
RainDrop Removal	Pix2pix [30]	*CVPR' 17*	28.02	0.85
	Attn.GAN [59]	*CVPR' 18*	30.55	0.90
	Quan et al. [63]	*ICCV' 19*	31.44	0.93
	CCN [62]	*CVPR' 21*	31.34	0.95
Multi-Tasks	All-in-One [41]	*CVPR' 20*	31.12	0.93
	TransWeather [69]	*CVPR' 22*	28.98	0.90
	Chen *et al*. [6]	*CVPR' 22*	30.75	0.91
	Ours	-	31.31	0.93

Table 4. **[Setting 1]** & **[Setting 2]** Comparisons on the SnowTest100k-L (S-L) dataset [51].

Type	Method	Venue	PSNR ↑	SSIM ↑
Desnowing	DetailsNet [17]	*CVPR' 17*	19.18	0.75
	DesnowNet [51]	*TIP' 18*	27.17	0.90
	JSTASR [4]	*ECCV' 20*	25.32	0.81
	DDMSNET [97]	*TIP' 21*	28.85	0.88
Multi-Tasks (Setting 1)	All-in-One [41]	*CVPR' 20*	28.33	0.88
	TransWeather [69]	*CVPR' 22*	27.80	0.85
	Chen *et al*. [6]	*CVPR' 22*	29.27	0.88
	Ours	-	29.71	0.89
Multi-Tasks (Setting 2)	TransWeather [69]	*CVPR' 22*	26.17	0.88
	Chen *et al*. [6]	*CVPR' 22*	28.71	0.88
	Ours	-	29.42	0.89

Table 5. **[Setting 2]** Comparisons on the RESIDE dataset [39].

Type	Method	Venue	PSNR ↑	SSIM ↑
Dehazing	EPDN [61]	*CVPR' 19*	23.82	0.89
	PFDN [14]	*ECCV' 20*	31.45	0.97
	KDDN [24]	*CVPR' 20*	33.49	0.97
	MSBDN [13]	*CVPR' 20*	33.79	0.98
	FFA-Net [60]	*AAAI' 20*	34.98	0.99
	AECRNet [77]	*CVPR' 21*	35.61	0.98
	MPRNet [92]	*CVPR' 21*	31.31	0.97
Multi-Tasks	All-in-One [41]	*CVPR' 20*	30.49	0.95
	TransWeather [69]	*CVPR' 22*	27.66	0.95
	Chen *et al*. [6]	*CVPR' 22*	30.76	0.97
	Ours	-	30.85	0.98

6.2. Benchmark Datasets

To verify the effectiveness of our method, we employ three dataset settings, which are presented in Tab. 1. Previous all-weather-removal methods [6, 41, 69] only perform their methods on the settings of the synthetic datasets, *e.g.*, **[Setting 1]** and **[Setting 2]**. Moreover, we construct the first

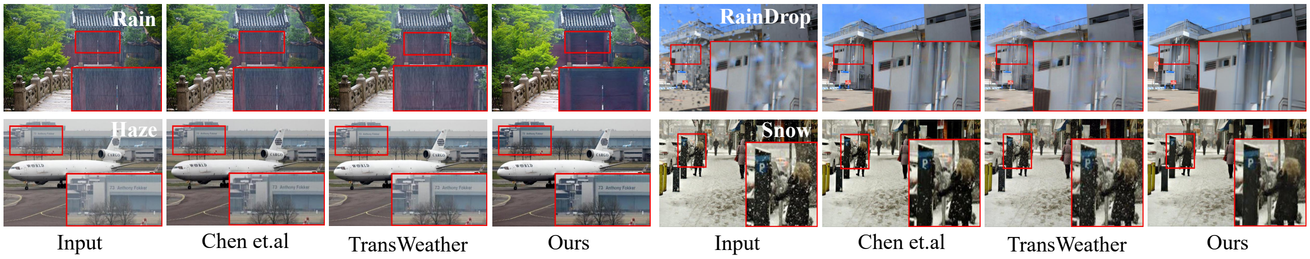

Figure 6. Visualization comparisons with previous all-weather-removal methods under multiple real-world weather conditions.

Table 6. **[Setting 2]** Comparisons on the Rain1400 dataset [17].

Type	Method	Venue	PSNR ↑	SSIM ↑
Deraining	JORDER [82]	*CVPR' 17*	31.28	0.92
	PReNet [64]	*CVPR' 19*	31.88	0.93
	DRD-Net [11]	*CVPR' 20*	29.65	0.88
	MSPFN [32]	*CVPR' 20*	29.24	0.88
	DualGCN [18]	*AAAI' 21*	30.50	0.91
	JRJG [88]	*CVPR' 21*	31.18	0.91
	MPRNet [92]	*CVPR' 21*	31.53	0.96
Multi Task	All-in-One [41]	*CVPR' 20*	30.82	0.90
	TransWeather [69]	*CVPR' 22*	29.14	0.89
	Chen *et al.* [6]	*CVPR' 22*	31.75	0.91
	Ours	-	32.49	0.93

Table 7. Comparisons results on the datasets of **[Setting 3]**.

Datasets	Method	Venue	PSNR ↑	SSIM ↑
SPA+	TransWeather [69]	*CVPR' 22*	33.64	0.93
	Chen *et al.* [6]	*CVPR' 22*	37.32	0.97
	Ours	-	38.94	0.98
RealSnow	TransWeather [69]	*CVPR' 22*	29.16	0.82
	Chen *et al.* [6]	*CVPR' 22*	29.37	0.88
	Ours	-	29.46	0.85
REVIDE [99]	TransWeather [69]	*CVPR' 22*	17.33	0.82
	Chen *et al.* [6]	*CVPR' 22*	20.10	0.85
	Ours	-	20.44	0.87

Table 8. Ablation study of our training strategy using the PNSR metric on the Datasets of **[Setting 1]**.

Models	Experiment settings	Rain	RainDrop	S-L
Model-1	Ours-Stage 1 (4.98 M)	25.04	30.88	29.13
Model-2	Ours-Stage 2 (5.97 M)	25.31	31.31	29.71
Model-3	Random Expansion of specific #Param.	25.14	30.96	29.28
Model-4	Enlarging #Param. of Model-1 (6.79 M)	25.22	30.99	29.42

Table 9. Ablation study of the parameters expansion types.

Type	Setting 1			Setting 2		
	Rain	RainDrop	S-L	Rain1400	RESIDE	S-L
1×1	30.31	31.31	29.71	32.49	30.85	29.43
3×3	30.52	31.52	29.86	32.75	30.90	29.69

real-world benchmark dataset for image restoration under multiple weather conditions of real scenes (**[Setting 3]**).

For fair comparisons, we follow [6,41] to uniformly sample images/patches from the dataset for network training. Meanwhile, except for *RealSnow* in **[Setting 3]**, we adopt the corresponding test datasets that have already been predivided by the pioneer works [17, 39, 40, 51, 59, 73].

Table 10. Ablation study of losses on the Datasets of **[Setting 1]**.

	$l_{content}$	l_{depth}	Outdoor-Rain	RainDrop	Snow100K-L
Stage 1	✓		24.96	30.79	29.00
	✓	✓	25.04	30.88	29.13

Table 11. Model efficiency comparisons.

Methods	All-in-One	Chen *et al.*	TransWeather	Ours
# Param (M: 10^6)	44.00	28.71	38.05	5.97
Inference Time (s)	-	0.067	0.026	0.030

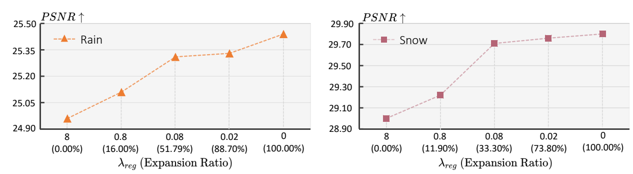

Figure 7. Ablation study of the regularization term λ_{reg} .

6.3. Comparison with the State-of-the-art Methods

Similar to [41, 69], we adopt the Peak Signal-to-Noise Ratio (PSNR) and the structural similarity (SSIM) [76] to evaluate the restoration performance of different models. PSNR and SSIM are calculated along the RGB channels.

In Tables 2 3 4 5 6 7, we report the qualitative comparison results among different methods, including both all-weather-removal and typical-weather-removal methods. Obviously, our method achieves superior performance in terms of all metrics on all datasets compared with all-weather-removal methods. In particular, our method surpasses TransWeather [69][1] by nearly two dB on multiple datasets under different weather conditions.

Moreover, we provide visual comparisons on the real-world scenarios of various kinds of weather in Fig. 6. It is evident that our results successfully preserve background details and remove multiple weather artifacts. In contrast, the apparent artifacts still exist in the results of [69].

6.4. Ablation Study

We further conduct ablation studies to validate the effects of each component in our method.

Ablation study of the two-stage training strategy. We set up three models with the following configurations: (i) Model-1 adopts the first training stage, and the network only learns the weather-general parameters; (ii) Model-2

[1]The authors have updated their results in the new arxiv version.

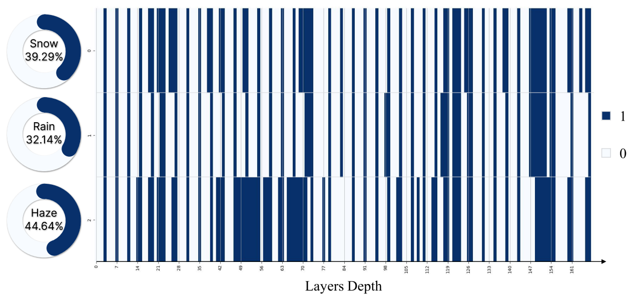

Figure 8. Visualization of the learned positions of expanded parameters. '1': expansion and '0': non-expansion.

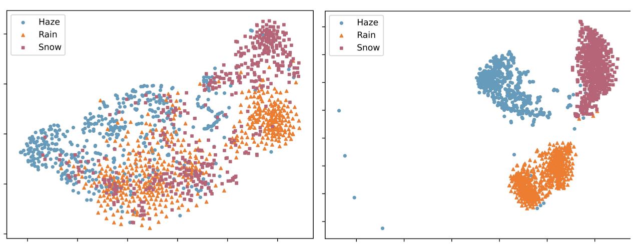

(a) t-SNE from weather-general features (b) t-SNE from weather-specific features

Figure 9. Visualization of t-SNE from learned weather-general and weather-specific features with our proposed training strategy.

adopts two training stages, and we fix the weather-general parameters and learn the weather-specific parameters; (iii) Model-4 expands the weather-specific parameters with the random sampling positions strategy. (iv) Model-4 enlarges the parameters of Model-1, and the network only learns the weather-general parameters.

As reported in Tab. 8, the performance of Model-2 performs is significantly improved after the second training stage, showing the effectiveness of our training strategy. For fair comparisons, note that Model-3 enlarges the network parameters by directly increasing the channel dimensions. Compared to Model-3 and Model-4, Model-2 adopts the adaptive parameters expansion strategy with fewer parameters but delivers better restoration performance.

Ablation study of expansion ratios. As described in Sec. 4.1, we introduce a sparsity regularization in the objective function during the second training stage. It guides our network to discover effective positions where to expand the weather-specific parameters. Consequently, the expansion ratio is defined as the ratio of the number of learned positions to the total number of positions. The expansion ratios mainly depend on the coefficient of the regularization term λ_{reg}. Consequently, we could adjust the λ_{reg} to achieve a trade-off between the model efficiency and the number of expansions. Using smaller λ_{reg} usually achieves better model performance while leading to larger expansion ratios. Meanwhile, larger expansion ratios often require more weather-specific parameters, bringing more computational overhead. In Fig.7, we present the model performance under different values of λ_{reg}. Considering the model efficiency, we set the default value of λ_{reg} as 0.08. Moreover, we visualize the learned positions in Fig.8. The middle layers have a stronger response to haze, since the middle features of the haze model are largely different from other weather types from Fig. 3.

Ablation study of the parameters expansion types. We also study two weather-specific parameter types: convolution layers with the kernel size of 3×3 and 1×1. As shown in Tab. 9, we report the performance of these two types under a similar expansion ratio condition. Obviously, given the similar expansion ratios of parameters, using 3×3 convolutions slightly performs better than the 1×1 convolutions but requires more network parameters. Hence, we adopt convolutions with kernel size of 1×1 as the default throughout the experiments.

Ablation study of losses. We validate the effectiveness of loss functions in Tab. 10, indicating that the auxiliary depth information improves the restoration performance.

Ablation study of feature representations. Fig. 9 visualizes the t-SNE results [70] of the weather-general and weather-specific features from the last layer of our network. It indicates that our strategy can learn uniformly weather-general and distinctively weather-specific features.

Efficiency comparisons. In Tab. 11, we further conduct comparisons of the network parameters and the average inference times among all-weather-removal methods. Our method uses much fewer network parameters than others but achieves better performance, as shown in Sec. 6.3. Moreover, our method only takes 0.03 seconds to process an image with the resolution of 256×256 on a single NVIDIA Geforce GTX 1080 Ti GPU.

7. Conclusion

This work formulates an efficiently unified model to remove weather-related artifacts under multiple adverse weather conditions. To achieve this, we design a two-stage training strategy, which first optimizes the network to learn weather-general features and then to learn the weather-specific features. More importantly, our method expands the network parameters to generate weather-specific features adaptively, thus reducing the computation overhead of our model. Moreover, we construct the first real-world dataset with multiple adverse weather conditions to promote the further research on the real-world scenarios. Various experiments demonstrate the superiority of our method over other state-of-the-art methods.

Acknowledgment. This work was supported in part by the National Natural Science Foundation of China (NSFC) under Grant 62276243, in part by the National Key R&D Program of China(NO.2022ZD0160100), and in part by Shanghai Committee of Science and Technology (Grant No. 21DZ1100100).

References

[1] Bolun Cai, Xiangmin Xu, Kui Jia, Chunmei Qing, and Dacheng Tao. DehazeNet: An end-to-end system for single image haze removal. *IEEE Trans. Image Process.*, 25(11):5187–5198, 2016. 1, 2, 3, 4

[2] Chenghao Chen and Hao Li. Robust representation learning with feedback for single image deraining. In *IEEE Conf. Comput. Vis. Pattern Recog.*, pages 7742–7751, 2021. 2

[3] Hanting Chen, Yunhe Wang, Tianyu Guo, Chang Xu, Yiping Deng, Zhenhua Liu, Siwei Ma, Chunjing Xu, Chao Xu, and Wen Gao. Pre-trained image processing transformer. In *IEEE Conf. Comput. Vis. Pattern Recog.*, pages 12299–12310, 2021. 3

[4] Wei-Ting Chen, Hao-Yu Fang, Jian-Jiun Ding, Cheng-Che Tsai, and Sy-Yen Kuo. JSTASR: Joint size and transparency-aware snow removal algorithm based on modified partial convolution and veiling effect removal. In *IEEE Eur. Conf. Comput. Vis.*, pages 754–770, 2020. 1, 2, 3, 4, 6

[5] Wei-Ting Chen, Hao-Yu Fang, Cheng-Lin Hsieh, Cheng-Che Tsai, I-Hsiang Chen, Jian-Jiun Ding, Sy-Yen Kuo, et al. All snow removed: Single image desnowing algorithm using hierarchical dual-tree complex wavelet representation and contradict channel loss. In *IEEE Int. Conf. Comput. Vis.*, pages 4196–4205, 2021. 3

[6] Wei-Ting Chen, Zhi-Kai Huang, Cheng-Che Tsai, Hao-Hsiang Yang, Jian-Jiun Ding, and Sy-Yen Kuo. Learning multiple adverse weather removal via two-stage knowledge learning and multi-contrastive regularization: Toward a unified model. In *IEEE Conf. Comput. Vis. Pattern Recog.*, pages 17653–17662, 2022. 1, 2, 3, 6, 7

[7] Xiang Chen, Jinshan Pan, Kui Jiang, Yufeng Li, Yufeng Huang, Caihua Kong, Longgang Dai, and Zhentao Fan. Unpaired deep image deraining using dual contrastive learning. In *IEEE Conf. Comput. Vis. Pattern Recog.*, pages 2017–2026, 2022. 2

[8] Zeyuan Chen, Yangchao Wang, Yang Yang, and Dong Liu. PSD: Principled synthetic-to-real dehazing guided by physical priors. In *IEEE Conf. Comput. Vis. Pattern Recog.*, pages 7180–7189, 2021. 3

[9] Corinna Cortes, Mehryar Mohri, and Afshin Rostamizadeh. Algorithms for learning kernels based on centered alignment. *J. Mach. Learn. Res.*, 13:795–828, 2012. 4

[10] Qili Deng, Ziling Huang, Chung-Chi Tsai, and Chia-Wen Lin. Hardgan: A haze-aware representation distillation gan for single image dehazing. In *Computer Vision–ECCV 2020: 16th European Conference, Glasgow, UK, August 23–28, 2020, Proceedings, Part VI 16*. Springer, 2020. 2

[11] Sen Deng, Mingqiang Wei, Jun Wang, Yidan Feng, Luming Liang, Haoran Xie, Fu Lee Wang, and Meng Wang. Detail-recovery image deraining via context aggregation networks. In *IEEE Conf. Comput. Vis. Pattern Recog.*, pages 14560–14569, 2020. 2, 7

[12] Zijun Deng, Lei Zhu, Xiaowei Hu, Chi-Wing Fu, Xuemiao Xu, Qing Zhang, Jing Qin, and Pheng-Ann Heng. Deep multi-model fusion for single-image dehazing. In *IEEE Int. Conf. Comput. Vis.*, pages 2453–2462, 2019. 2

[13] Hang Dong, Jinshan Pan, Lei Xiang, Zhe Hu, Xinyi Zhang, Fei Wang, and Ming-Hsuan Yang. Multi-scale boosted dehazing network with dense feature fusion. In *IEEE Conf. Comput. Vis. Pattern Recog.*, pages 2157–2167, 2020. 3, 6

[14] Jiangxin Dong and Jinshan Pan. Physics-based feature dehazing networks. In *IEEE Eur. Conf. Comput. Vis.*, pages 188–204. Springer, 2020. 6

[15] David Eigen, Dilip Krishnan, and Rob Fergus. Restoring an image taken through a window covered with dirt or rain. In *IEEE Int. Conf. Comput. Vis.*, pages 633–640, 2013. 2

[16] Xueyang Fu, Jiabin Huang, Xinghao Ding, Yinghao Liao, and John Paisley. Clearing the skies: A deep network architecture for single-image rain removal. *IEEE Trans. Image Process.*, 26(6):2944–2956, 2017. 1, 2

[17] Xueyang Fu, Jiabin Huang, Delu Zeng, Yue Huang, Xinghao Ding, and John Paisley. Removing rain from single images via a deep detail network. In *IEEE Conf. Comput. Vis. Pattern Recog.*, pages 3855–3863, 2017. 1, 2, 6, 7

[18] Xueyang Fu, Qi Qi, Zheng-Jun Zha, Yurui Zhu, and Xinghao Ding. Rain streak removal via dual graph convolutional network. In *Proc. AAAI Conf. Artif. Intell.*, volume 35, pages 1352–1360, 2021. 7

[19] Xueyang Fu, Jie Xiao, Yurui Zhu, Aiping Liu, Feng Wu, and Zheng-Jun Zha. Continual image deraining with hypergraph convolutional networks. *IEEE Transactions on Pattern Analysis and Machine Intelligence*, 2023. 2

[20] Chun-Le Guo, Qixin Yan, Saeed Anwar, Runmin Cong, Wenqi Ren, and Chongyi Li. Image dehazing transformer with transmission-aware 3D position embedding. In *IEEE Conf. Comput. Vis. Pattern Recog.*, pages 5812–5820, 2022. 3

[21] Xin Guo, Xueyang Fu, Man Zhou, Zhen Huang, Jialun Peng, and Zheng-Jun Zha. Exploring fourier prior for single image rain removal. In *Proceedings of the 30th International Joint Conferences on Artificial Intelligence*, pages 935–941, 2022. 2

[22] Zhixiang Hao, Shaodi You, Yu Li, Kunming Li, and Feng Lu. Learning from synthetic photorealistic raindrop for single image raindrop removal. In *IEEE Int. Conf. Comput. Vis.*, Oct 2019. 1, 2

[23] Kaiming He, Jian Sun, and Xiaoou Tang. Single image haze removal using dark channel prior. *IEEE Trans. Pattern Anal. Mach. Intell.*, 33(12):2341–2353, 2010. 1, 2, 3

[24] Ming Hong, Yuan Xie, Cuihua Li, and Yanyun Qu. Distilling image dehazing with heterogeneous task imitation. In *IEEE Conf. Comput. Vis. Pattern Recog.*, pages 3462–3471, 2020. 6

[25] Xiaowei Hu, Chi-Wing Fu, Lei Zhu, and Pheng-Ann Heng. Depth-attentional features for single-image rain removal. In *IEEE Conf. Comput. Vis. Pattern Recog.*, pages 8022–8031, 2019. 1, 2

[26] Xiaowei Hu, Lei Zhu, Tianyu Wang, Chi-Wing Fu, and Pheng-Ann Heng. Single-image real-time rain removal based on depth-guided non-local features. *IEEE Trans. Image Process.*, 30:1759–1770, 2021. 2

[27] Huaibo Huang, Aijing Yu, and Ran He. Memory oriented transfer learning for semi-supervised image deraining. In

IEEE Conf. Comput. Vis. Pattern Recog., pages 7732–7741, 2021. 2

[28] Jie Huang, Yajing Liu, Feng Zhao, Keyu Yan, Jinghao Zhang, Yukun Huang, Man Zhou, and Zhiwei Xiong. Deep fourier-based exposure correction network with spatial-frequency interaction. In *ECCV*. Springer, 2022. 2

[29] Jie Huang, Man Zhou, Yajing Liu, Mingde Yao, Feng Zhao, and Zhiwei Xiong. Exposure-consistency representation learning for exposure correction. In *Proceedings of the 30th ACM International Conference on Multimedia*, page 6309–6317, 2022. 2

[30] Phillip Isola, Jun-Yan Zhu, Tinghui Zhou, and Alexei A Efros. Image-to-image translation with conditional adversarial networks. In *IEEE Conf. Comput. Vis. Pattern Recog.*, pages 1125–1134, 2017. 6

[31] Da-Wei Jaw, Shih-Chia Huang, and Sy-Yen Kuo. Desnow-Gan: An efficient single image snow removal framework using cross-resolution lateral connection and GANs. *IEEE Trans. Circuits Syst. Video Technol.*, 31(4):1342–1350, 2020. 3

[32] Kui Jiang, Zhongyuan Wang, Peng Yi, Chen Chen, Baojin Huang, Yimin Luo, Jiayi Ma, and Junjun Jiang. Multi-scale progressive fusion network for single image deraining. In *IEEE Conf. Comput. Vis. Pattern Recog.*, pages 8346–8355, 2020. 2, 7

[33] Justin Johnson, Alexandre Alahi, and Li Fei-Fei. Perceptual losses for real-time style transfer and super-resolution. In *IEEE Eur. Conf. Comput. Vis.*, pages 694–711. Springer, 2016. 5

[34] Jin-Hwan Kim, Jae-Young Sim, and Chang-Su Kim. Single image dehazing based on contrast enhancement. In *2011 IEEE Int. Conf. on Acoustics, Speech and Signal Processing*, pages 1273–1276. IEEE, 2011. 2

[35] Diederik P. Kingma and Jimmy Ba. Adam: A method for stochastic optimization. *CoRR*, abs/1412.6980, 2015. 6

[36] Simon Kornblith, Mohammad Norouzi, Honglak Lee, and Geoffrey Hinton. Similarity of neural network representations revisited. In *Proc. Int. Conf. Mach. Learn.*, pages 3519–3529. PMLR, 2019. 4

[37] Simon Kornblith, Jonathon Shlens, and Quoc V Le. Do better ImageNet models transfer better? In *IEEE Conf. Comput. Vis. Pattern Recog.*, pages 2661–2671, 2019. 4

[38] Boyi Li, Xiulian Peng, Zhangyang Wang, Jizheng Xu, and Dan Feng. Aod-net: All-in-one dehazing network. In *IEEE Int. Conf. Comput. Vis.*, pages 4770–4778, 2017. 3

[39] Boyi Li, Wenqi Ren, Dengpan Fu, Dacheng Tao, Dan Feng, Wenjun Zeng, and Zhangyang Wang. Benchmarking single-image dehazing and beyond. *IEEE Trans. Image Process.*, 28(1):492–505, 2019. 4, 6, 7

[40] Ruoteng Li, Loong-Fah Cheong, and Robby T. Tan. Heavy rain image restoration: Integrating physics model and conditional adversarial learning. In *IEEE Conf. Comput. Vis. Pattern Recog.*, pages 1633–1642, 2019. 1, 2, 6, 7

[41] Ruoteng Li, Robby T. Tan, and Loong-Fah Cheong. All in one bad weather removal using architectural search. In *IEEE Conf. Comput. Vis. Pattern Recog.*, pages 3175–3185, 2020. 1, 2, 3, 6, 7

[42] Wenbo Li, Xin Lu, Jiangbo Lu, Xiangyu Zhang, and Jiaya Jia. On efficient transformer and image pre-training for low-level vision. *arXiv preprint arXiv:2112.10175*, 2021. 3, 4

[43] Xia Li, Jianlong Wu, Zhouchen Lin, Hong Liu, and Hongbin Zha. Recurrent squeeze-and-excitation context aggregation net for single image deraining. In *IEEE Eur. Conf. Comput. Vis.*, pages 254–269, 2018. 2

[44] Yi Li, Yi Chang, Yan Gao, Changfeng Yu, and Luxin Yan. Physically disentangled intra-and inter-domain adaptation for varicolored haze removal. In *IEEE Conf. Comput. Vis. Pattern Recog.*, pages 5841–5850, 2022. 3

[45] Yunan Li, Qiguang Miao, Wanli Ouyang, Zhenxin Ma, Huijuan Fang, Chao Dong, and Yining Quan. Lap-net: Level-aware progressive network for image dehazing. In *Proceedings of the IEEE/CVF International Conference on Computer Vision*, 2019. 2

[46] Huan Liu, Zijun Wu, Liangyan Li, Sadaf Salehkalaibar, Jun Chen, and Keyan Wang. Towards multi-domain single image dehazing via test-time training. In *IEEE Conf. Comput. Vis. Pattern Recog.*, pages 5831–5840, 2022. 3

[47] Lina Liu, Xibin Song, Mengmeng Wang, Yong Liu, and Liangjun Zhang. Self-supervised monocular depth estimation for all day images using domain separation. In *IEEE Int. Conf. Comput. Vis.*, pages 12737–12746, 2021. 5

[48] Pengfei Liu, Xipeng Qiu, and Xuanjing Huang. Recurrent neural network for text classification with multi-task learning. *arXiv preprint arXiv:1605.05101*, 2016. 3

[49] Xiaohong Liu, Yongrui Ma, Zhihao Shi, and Jun Chen. GridDehazeNet: Attention-based multi-scale network for image dehazing. In *IEEE Int. Conf. Comput. Vis.*, pages 7314–7323, 2019. 1, 2, 3

[50] Yang Liu, Jinshan Pan, Jimmy Ren, and Zhixun Su. Learning deep priors for image dehazing. In *Proceedings of the IEEE/CVF international conference on computer vision*, 2019. 2

[51] Yun-Fu Liu, Da-Wei Jaw, Shih-Chia Huang, and Jenq-Neng Hwang. DesnowNet: Context-aware deep network for snow removal. *IEEE Trans. Image Process.*, 27(6):3064–3073, 2018. 1, 2, 3, 6, 7

[52] Ilya Loshchilov and Frank Hutter. SGDR: Stochastic gradient descent with warm restarts. In *International Conference on Learning Representations*, 2017. 6

[53] Jiayuan Mao, Tete Xiao, Yuning Jiang, and Zhimin Cao. What can help pedestrian detection? In *IEEE Conf. Comput. Vis. Pattern Recog.*, 2017. 1

[54] Srinivasa G. Narasimhan. *Models and algorithms for vision through the atmosphere*. Columbia University, 2004. 3

[55] Srinivasa G. Narasimhan and Shree K. Nayar. Vision and the atmosphere. *Int. J. Comput. Vis.*, 48(3):233–254, 2002. 2, 3

[56] Shree K Nayar and Srinivasa G. Narasimhan. Vision in bad weather. In *IEEE Int. Conf. Comput. Vis.*, volume 2, pages 820–827. IEEE, 1999. 3

[57] Shree K. Nayar and Srinivasa G. Narasimhan. Seeing through bad weather. In *Int. Symp. Robot. Res.*, pages 335–350. Springer, 2005. 2, 3

[58] Thao Nguyen, Maithra Raghu, and Simon Kornblith. Do wide and deep networks learn the same things? uncovering how neural network representations vary with width and depth. *arXiv preprint arXiv:2010.15327*, 2020. 4

[59] Rui Qian, Robby T. Tan, Wenhan Yang, Jiajun Su, and Jiaying Liu. Attentive generative adversarial network for raindrop removal from a single image. In *IEEE Conf. Comput. Vis. Pattern Recog.*, pages 2482–2491, 2018. 1, 2, 6, 7

[60] Xu Qin, Zhilin Wang, Yuanchao Bai, Xiaodong Xie, and Huizhu Jia. FFA-Net: Feature fusion attention network for single image dehazing. In *Proc. AAAI Conf. Artif. Intell.*, volume 34, pages 11908–11915, 2020. 6

[61] Yanyun Qu, Yizi Chen, Jingying Huang, and Yuan Xie. Enhanced pix2pix dehazing network. In *IEEE Conf. Comput. Vis. Pattern Recog.*, pages 8160–8168, 2019. 3, 6

[62] Ruijie Quan, Xin Yu, Yuanzhi Liang, and Yi Yang. Removing raindrops and rain streaks in one go. In *IEEE Conf. Comput. Vis. Pattern Recog.*, pages 9147–9156, 2021. 2, 6

[63] Yuhui Quan, Shijie Deng, Yixin Chen, and Hui Ji. Deep learning for seeing through window with raindrops. In *IEEE Int. Conf. Comput. Vis.*, pages 2463–2471, 2019. 2, 6

[64] Dongwei Ren, Wangmeng Zuo, Qinghua Hu, Pengfei Zhu, and Deyu Meng. Progressive image deraining networks: A better and simpler baseline. In *IEEE Conf. Comput. Vis. Pattern Recog.*, pages 3937–3946, 2019. 7

[65] Wenqi Ren, Si Liu, Hua Zhang, Jinshan Pan, Xiaochun Cao, and Ming-Hsuan Yang. Single image dehazing via multi-scale convolutional neural networks. In *IEEE Eur. Conf. Comput. Vis.*, pages 154–169. Springer, 2016. 1, 2, 3

[66] Wenqi Ren, Lin Ma, Jiawei Zhang, Jinshan Pan, Xiaochun Cao, Wei Liu, and Ming-Hsuan Yang. Gated fusion network for single image dehazing. In *IEEE Conf. Comput. Vis. Pattern Recog.*, pages 3253–3261, 2018. 3

[67] Olaf Ronneberger, Philipp Fischer, and Thomas Brox. U-Net: Convolutional networks for biomedical image segmentation. In *Proc. Int. Conf. Med. Image Comput. Comput.-Assisted Intervention*, pages 234–241. Springer, 2015. 4

[68] Robby T. Tan. Visibility in bad weather from a single image. In *IEEE Conf. Comput. Vis. Pattern Recog.*, pages 1–8. IEEE, 2008. 4

[69] Jeya Maria Jose Valanarasu, Rajeev Yasarla, and Vishal M. Patel. TransWeather: Transformer-based restoration of images degraded by adverse weather conditions. In *IEEE Conf. Comput. Vis. Pattern Recog.*, pages 2353–2363, 2022. 1, 2, 3, 6, 7

[70] Laurens Van der Maaten and Geoffrey Hinton. Visualizing data using t-SNE. *J. Mach. Learn. Res.*, 2008. 8

[71] Matthew Wallingford, Hao Li, Alessandro Achille, Avinash Ravichandran, Charless Fowlkes, Rahul Bhotika, and Stefano Soatto. Task adaptive parameter sharing for multi-task learning. In *IEEE Conf. Comput. Vis. Pattern Recog.*, pages 7561–7570, 2022. 3

[72] Hong Wang, Qi Xie, Qian Zhao, and Deyu Meng. A model-driven deep neural network for single image rain removal. In *IEEE Conf. Comput. Vis. Pattern Recog.*, pages 3103–3112, 2020. 1, 2

[73] Tianyu Wang, Xin Yang, Ke Xu, Shaozhe Chen, Qiang Zhang, and Rynson W.H. Lau. Spatial attentive single-image deraining with a high quality real rain dataset. In *IEEE Conf. Comput. Vis. Pattern Recog.*, pages 12270–12279, 2019. 1, 2, 5, 6, 7

[74] Yinglong Wang, Chao Ma, and Bing Zeng. Multi-decoding deraining network and quasi-sparsity based training. In *IEEE Conf. Comput. Vis. Pattern Recog.*, pages 13375–13384, 2021. 2

[75] Yinglong Wang, Yibing Song, Chao Ma, and Bing Zeng. Rethinking image deraining via rain streaks and vapors. In *IEEE Eur. Conf. Comput. Vis.*, pages 367–382. Springer, 2020. 4

[76] Zhou Wang, Alan C Bovik, Hamid R Sheikh, and Eero P. Simoncelli. Image quality assessment: from error visibility to structural similarity. *IEEE Trans. Image Process.*, 13(4):600–612, 2004. 7

[77] Haiyan Wu, Yanyun Qu, Shaohui Lin, Jian Zhou, Ruizhi Qiao, Zhizhong Zhang, Yuan Xie, and Lizhuang Ma. Contrastive learning for compact single image dehazing. In *IEEE Conf. Comput. Vis. Pattern Recog.*, pages 10551–10560, 2021. 3, 6

[78] Jie Xiao, Xueyang Fu, Aiping Liu, Feng Wu, and Zheng-Jun Zha. Image de-raining transformer. *IEEE Trans. Pattern Anal. Mach. Intell.*, pages 1–18, 2022. 2

[79] Jie Xiao, Man Zhou, Xueyang Fu, Aiping Liu, and Zheng-Jun Zha. Improving de-raining generalization via neural reorganization. In *IEEE Int. Conf. Comput. Vis.*, pages 4987–4996, 2021. 2

[80] Dong Yang and Jian Sun. Proximal Dehaze-Net: A prior learning-based deep network for single image dehazing. In *IEEE Eur. Conf. Comput. Vis.*, pages 702–717, 2018. 1, 2, 3

[81] Wenhan Yang, Robby T. Tan, Jiashi Feng, Zongming Guo, Shuicheng Yan, and Jiaying Liu. Joint rain detection and removal from a single image with contextualized deep networks. *IEEE Trans. Pattern Anal. Mach. Intell.*, 42(6):1377–1393, 2019. 2, 4

[82] Wenhan Yang, Robby T. Tan, Jiashi Feng, Jiaying Liu, Zongming Guo, and Shuicheng Yan. Deep joint rain detection and removal from a single image. In *IEEE Conf. Comput. Vis. Pattern Recog.*, pages 1357–1366, 2017. 1, 2, 7

[83] Wenhan Yang, Robby T. Tan, Shiqi Wang, Yuming Fang, and Jiaying Liu. Single image deraining: From model-based to data-driven and beyond. *IEEE Trans. Pattern Anal. Mach. Intell.*, 43(11):4059–4077, 2020. 1, 2

[84] Xitong Yang, Zheng Xu, and Jiebo Luo. Towards perceptual image dehazing by physics-based disentanglement and adversarial training. In *Proc. AAAI Conf. Artif. Intell.*, volume 32, 2018. 1, 2, 3

[85] Yang Yang, Chaoyue Wang, Risheng Liu, Lin Zhang, Xiaojie Guo, and Dacheng Tao. Self-augmented unpaired image dehazing via density and depth decomposition. In *IEEE Conf. Comput. Vis. Pattern Recog.*, pages 2037–2046, 2022. 3

[86] Zizheng Yang, Mingde Yao, Jie Huang, Man Zhou, and Feng Zhao. Sir-former: Stereo image restoration using

transformer. In *Proceedings of the 30th ACM International Conference on Multimedia*, page 6377–6385, 2022. 2

[87] Rajeev Yasarla, Vishwanath A. Sindagi, and Vishal M. Patel. Syn2real transfer learning for image deraining using gaussian processes. In *IEEE Conf. Comput. Vis. Pattern Recog.*, pages 2726–2736, 2020. 2

[88] Yuntong Ye, Yi Chang, Hanyu Zhou, and Luxin Yan. Closing the loop: Joint rain generation and removal via disentangled image translation. In *IEEE Conf. Comput. Vis. Pattern Recog.*, pages 2053–2062, 2021. 7

[89] Qiaosi Yi, Juncheng Li, Qinyan Dai, Faming Fang, Guixu Zhang, and Tieyong Zeng. Structure-preserving deraining with residue channel prior guidance. In *IEEE Int. Conf. Comput. Vis.*, pages 4238–4247, 2021. 2

[90] Hu Yu, Jie Huang, Yajing Liu, Qi Zhu, Man Zhou, and Feng Zhao. Source-free domain adaptation for real-world image dehazing. In *Proceedings of the 30th ACM International Conference on Multimedia*, page 6645–6654, 2022. 2

[91] Ye Yuntong, Yu Changfeng, Chang Yi, Zhu Lin, Zhao Xile, Yan Luxin, and Tian Yonghong. Unsupervised deraining: Where contrastive learning meets self-similarity. *arXiv preprint arXiv:2203.11509*, 2022. 2

[92] Syed Waqas Zamir, Aditya Arora, Salman Khan, Munawar Hayat, Fahad Shahbaz Khan, Ming-Hsuan Yang, and Ling Shao. Multi-stage progressive image restoration. In *IEEE Conf. Comput. Vis. Pattern Recog.*, pages 14821–14831, 2021. 6, 7

[93] He Zhang and Vishal M. Patel. Densely connected pyramid dehazing network. In *IEEE Conf. Comput. Vis. Pattern Recog.*, pages 3194–3203, 2018. 3

[94] He Zhang, Vishwanath Sindagi, and Vishal M. Patel. Image de-raining using a conditional generative adversarial network. *IEEE Trans. Circuits Syst. Video Technol.*, 30(11):3943–3956, 2019. 2

[95] Jinghao Zhang, Jie Huang, Mingde Yao, Man Zhou, and Feng Zhao. Structure- and texture-aware learning for low-light image enhancement. In *Proceedings of the 30th ACM International Conference on Multimedia*, page 6483–6492, 2022. 2

[96] Kaihao Zhang, Dongxu Li, Wenhan Luo, and Wenqi Ren. Dual attention-in-attention model for joint rain streak and raindrop removal. *IEEE Trans. Image Process.*, 30:7608–7619, 2021. 1, 2

[97] Kaihao Zhang, Rongqing Li, Yanjiang Yu, Wenhan Luo, and Changsheng Li. Deep dense multi-scale network for snow removal using semantic and depth priors. *IEEE Trans. Image Process.*, 30:7419–7431, 2021. 1, 2, 3, 6

[98] Kaihao Zhang, Wenhan Luo, Wenqi Ren, Jingwen Wang, Fang Zhao, Lin Ma, and Hongdong Li. Beyond monocular deraining: Stereo image deraining via semantic understanding. In *Computer Vision–ECCV 2020: 16th European Conference, Glasgow, UK, August 23–28, 2020, Proceedings, Part XXVII 16*. Springer, 2020. 2

[99] Xinyi Zhang, Hang Dong, Jinshan Pan, Chao Zhu, Ying Tai, Chengjie Wang, Jilin Li, Feiyue Huang, and Fei Wang. Learning to restore hazy video: A new real-world dataset and a new method. In *IEEE Conf. Comput. Vis. Pattern Recog.*, pages 9239–9248, June 2021. 5, 6, 7

[100] Yu Zhang and Qiang Yang. An overview of multi-task learning. *Natl. Sci*, 5(1):30–43, 2018. 3

[101] Zheyu Zhang, Yurui Zhu, Xueyang Fu, Zhiwei Xiong, Zheng-Jun Zha, and Feng Wu. Multifocal attention-based cross-scale network for image de-raining. In *Proceedings of the 29th ACM International Conference on Multimedia*, pages 3673–3681, 2021. 2

[102] Zhuoran Zheng, Wenqi Ren, Xiaochun Cao, Xiaobin Hu, Tao Wang, Fenglong Song, and Xiuyi Jia. Ultra-high-definition image dehazing via multi-guided bilateral learning. In *IEEE Conf. Comput. Vis. Pattern Recog.*, pages 16180–16189. IEEE, 2021. 3

[103] Man Zhou, Jie Huang, Keyu Yan, Hu Yu, Xueyang Fu, Aiping Liu, Xian Wei, and Feng Zhao. Spatial-frequency domain information integration for pan-sharpening. In *ECCV*. Springer, 2022. 2

[104] Man Zhou, Jie Xiao, Yifan Chang, Xueyang Fu, Aiping Liu, Jinshan Pan, and Zheng-Jun Zha. Image de-raining via continual learning. In *IEEE Conf. Comput. Vis. Pattern Recog.*, pages 4907–4916, 2021. 2

[105] Kai Zhu, Wei Zhai, Yang Cao, Jiebo Luo, and Zheng-Jun Zha. Self-sustaining representation expansion for non-exemplar class-incremental learning. In *IEEE Conf. Comput. Vis. Pattern Recog.*, pages 9296–9305, 2022. 3

[106] Lei Zhu, Zijun Deng, Xiaowei Hu, Haoran Xie, Xuemiao Xu, Jing Qin, and Pheng-Ann Heng. Learning gated non-local residual for single-image rain streak removal. *IEEE Trans. Circuits Syst. Video Technol.*, 31(6):2147–2159, 2020. 2

[107] Zhe Zhu, Dun Liang, Songhai Zhang, Xiaolei Huang, Baoli Li, and Shimin Hu. Traffic-sign detection and classification in the wild. In *IEEE Conf. Comput. Vis. Pattern Recog.*, 2016. 1